Hindawi
Shock and Vibration
Volume 2019, Article ID 7938491, 16 pages
https://doi.org/10.1155/2019/7938491

Research Article

A Control Method of Rock Burst for Dynamic Roadway Floor in Deep Mining Mine

Zhimin Xiao,[1,2,3] **Jun Liu**,[1,2,3] **Shitan Gu**,[4,5] **Mingqing Liu**,[1,2,3] **Futian Zhao**,[1,2,3] **Yue Wang**,[1,2,3] **Chen Ou**,[1,2,3] **and Mengyang Zhen**[1,2,3]

[1]*College of Civil and Transportation Engineering, Hohai University, Nanjing 210098, China*
[2]*Institute of Engineering Safety and Disaster Prevention, Hohai University, Nanjing 210098, China*
[3]*Key Laboratory of Ministry of Education for Geomechanics and Embankment Engineering, Hohai University, Nanjing 210098, China*
[4]*State Key Laboratory of Mining Disaster Prevention and Control Co-Founded by Shandong Province and the Ministry of Science and Technology, Shandong University of Science and Technology, Qingdao, Shandong 266590, China*
[5]*College of Mining and Safety Engineering, Shandong University of Science and Technology, Qingdao, Shandong 266590, China*

Correspondence should be addressed to Zhimin Xiao; sdustxiaozhimin@163.com

Received 21 February 2019; Revised 26 May 2019; Accepted 27 June 2019; Published 21 August 2019

Academic Editor: Mohammad A. Hariri-Ardebili

Roadway floor rock burst is an important manifestation of rock bursts in deeply buried mines. With the increase of mining depth and mining intensity, rock burst disasters in the roadway floor such as floor heaves are becoming more serious. The article investigated the roadway floor severe heave caused by floor rock burst during excavation of the No. 3401 working face, which was controlled by an anticlinal structure and deep mining in Shandong Mine, China. Firstly, by analyzing geological conditions of the working face, roadway support parameters, and characteristics of coal and rock, it was revealed that high tectonic stress and high crustal stress were main causes of the floor rock burst. Secondly, based on the Theory of Mechanics and Theory of Energy, the energy conversion process in the roadway floor was discussed, and the rock burst condition caused by elastic energy in the roadway floor was analyzed. The failure characteristics of roadway-surrounding rock were also inspected, using a borehole recorder. The roof and sidewalls of roadway mainly contained fissures and cracks, whereas cracks and broken areas are distributed in the roadway floor. Finally, based on the deformation and failure characteristics of roadway-surrounding rock, a method termed "overbreaking-bolting and grouting-backfill" was proposed to control roadway floor rock burst. The method was tested in the field, and the results showed that it could effectively control the deformation of roadway floor and rock burst, guaranteeing the stability of roadway floor. This impact control method for the roadway floor can provide a reference for the prevention and control of roadway rock burst in mines with similar geological conditions.

1. Introduction

Rock burst, a special form of mine stress, can be described as an instantaneous release of high-strength coal (rock) strain elastic energy induced by mining. Vibrations in the surrounding rock and coal-rock extruding phenomenon occur in the corresponding mining space [1]. Since 1738, rock bursts have been reported in the leading coal mining countries, including the United Kingdom, Poland, South Africa, Russia, United States, and China [2–4]. With the increase of mining depths, frequency of rock bursts in mines increases significantly and the severity of resulting disasters is also increasing. According to the available statistics, there are more than 130 mines in China, and hundreds of casualties die every year from rock burst [5]. An investigation showed that 75% of rock burst accidents occurred in roadways [6, 7]. Consequently, the mechanism and control techniques of rock burst have been studied extensively by experts and scholars.

Based on the mechanical characteristics of coal rock and characteristics of rock burst, many experts have studied the disaster from three angles: the mechanism, early warning, and prevention and control.

Many scholars have conducted in-depth research on the mechanism and prevention of rock burst and made remarkable achievements. A series of theories, such as the Energy Theory, Stiffness Theory, Strength Theory, and Impact Tendencies Theory, have been put forward [8–11]. With the development of modern mathematics and computer technology, rock burst theories began to be investigated at the end of the 1970s. Based on the catastrophe theory [12–14], the damage propagation capacity of coal and rock mass was studied and the mechanism of rock burst was explored. Xie et al. [15] introduced fractal geometry into the study of rock burst, while Qi et al. [16] proposed the "three-factor" theory for studying the relationship between rock burst and coal-rock sliding failure. In the roadway rock burst theory, Ma et al. [17] discussed the mechanism and conditions of "butterfly" rock burst and put forward the "three criteria of rock burst," providing a new method for its prevention and control. Yang et al. [18] obtained that passive acoustic emissions monitoring systems coupled with double-difference tomography were capable of monitoring and forecasting failure of rock, for helping improve the safety and efficiency of mining projects. Jiang et al. [19] obtained that the intermediate principal stress has a significant effect on rock burst behavior of marble. Xu et al. [20] discussed the characteristics of roadway rock burst and put forward the concept of "roadway floor risk factor." Gu et al. [21] studied on rock burst risk induced by mining and field case.

Rock burst warning is an important part of rock burst prevention and control, and many scholars have conducted long-term research and put forward a variety of rock burst danger prediction and forecasting methods. At present, early-warning methods for rock burst mainly include the microseismic method, electromagnetic radiation method, acoustic emission method, and borehole method [22–24]. On the topic of microseismic monitoring and early warning, Husen et al. [25] discussed the seismicity caused by stress redistribution during the excavation of the MFS Faido, the southernmost access point in the new Gotthard Base Tunnel. Zhao et al. [26] studied the characteristics of rock burst microseismic signals under a hard coal seam and hard roof. Sharp decreases in microseismic frequency and an obvious increase in amplitude were regarded as characteristic of rock burst precursors. Cao et al. [27] studied the microseismic precursory characteristics of rock burst hazard and assessed rock burst risk and rock burst risk areas in coal mining. On electromagnetic emission forecasting technology, He et al. [28] used electromagnetic forecasting's pulse number and intensity as two indicators to classify danger of dynamical disasters into three levels of forecasting such as no danger, weak danger, and strong danger.

With regard to the prevention and control of rock burst, Pan et al. [29] put forward two roadway support designs to improve support stiffness and energy absorption. Kang et al. [30] insisted that the essence of rock burst roadway support is maintaining the integrity of the surrounding rock, forming a supporting stress field and bringing into play the anti-impact capacity of the surrounding rock. Li et al. [31] proposed an optimized roadway layout for effective control of gob-side rock bursts in the longwall mining of a thick coal seam. Raju et al. [32] proposed methodology for designing dynamic rock supports by estimating the stored energy around the Canada Mine. Feng et al. [33] presented coal burst mitigation strategy for tailgate during deep mining of inclined longwall top coal caving panels by analyzing field data and numerical simulation results.

However, with the increasing depth of coal mining, deep coal and rock mass are exposed by mining activities, and it can show complex geological characteristics and mechanical properties. Therefore, mining activities are more likely to induce severe and abrupt rock burst. In the article, the No. 3401 working face (in Shandong Mine, China) roadway floor heave induced by rock burst was studied as an example. First, the stability and energy laws of roadway floor were studied by using theoretical analysis and microseismic monitoring. Then, the internal failure characteristics of roadway-surrounding rock are determined and studied by using a borehole recorder. Finally, according to the deformation and failure characteristics of roadway floor, the "overbreaking-bolting and grouting-backfill" method was proposed. This method can improve the lithology of roadway floor, thus effectively controlling roadway floor deformation and guaranteeing roadway stability.

2. Rock Burst Manifestation of the Roadway Floor

2.1. Engineering Geological Characteristics of Working Face. The No. 3401 working face is the first working face in the No. 4 mining area in Shandong Mine, China, and the mining seam belongs to No. 3 coal seam. The working face elevation is −986 m to −914 m, corresponding to the ground elevation of +52.86 m to +54.75 m, and the average buried depth of working face is 1000 m, which is classified as a deep mining face. The average thickness of coal seam is 4.7 m, and it is affected by an anticlinal structure. The working face layout is shown in Figure 1. Based on the 15 boreholes in the mine fine-searching stage, macroscopic structure of the No. 3 coal seam is plotted in Figure 2. These boreholes only have boreholes No. T9-6 and No. T10-3 passing through No. 3401 working face.

Figures 1 and 2 show that overall occurrence status of the No. 3 coal mine is controlled by the fold structure. The anticlinal structure greatly influences the No. 3 coal seam uplift, while the influence of synclinal structure is relatively small. The coal seam in the No. 3401 working face is greatly influenced by the anticline, and the geostress is large. Therefore, roadway excavation activity further increases the possibility of rock burst. Table 1 shows the results of a geostress test in the mining area.

Table 1 shows that geostress is mainly controlled by horizontal stress and that direction of the maximum

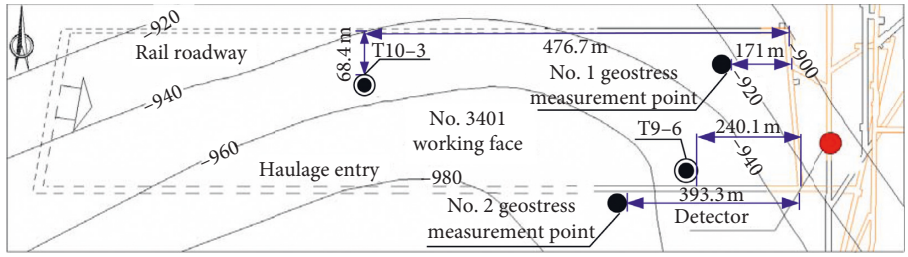

Figure 1: Layout of No. 3401 working face.

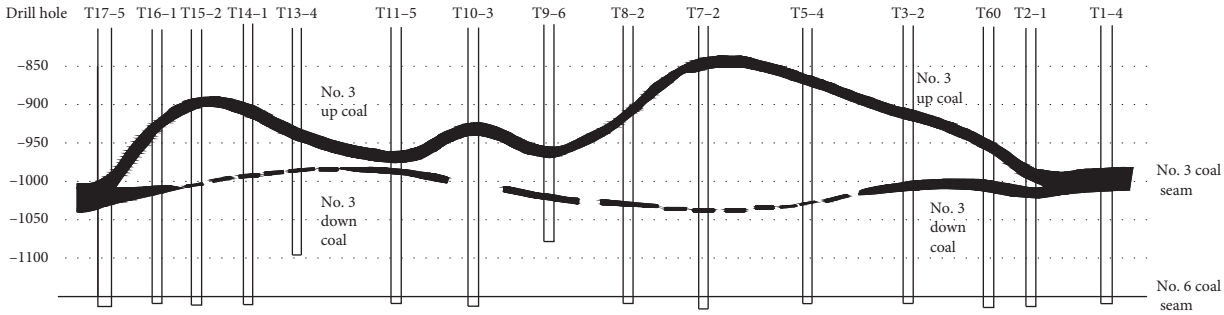

Figure 2: Macroscopic storage structure profile of No. 3 coal seam.

Table 1: Results of geostress measurement.

No.	Monitoring station	Depth (m)	Vertical principal stress (σ_v/MPa)	Maximum horizontal principal stress (σ_H/MPa)	Minimum horizontal principal stress (σ_H/MPa)	Maximum horizontal principal stress direction
1	First station	1040	27.67	51.17	27.11	N22.3°E
2	Second station	964	25.55	49.57	27.59	N31.2°E
3	Third station	967	25.64	49.74	26.15	N25.5°E
4	Fourth station	982	26.10	50.9	26.88	N20.1°E
5	Fifth station	1034	27.30	49.4	26.75	N35.7°E

principal stress is from N20.1 E to N35.7 E, which has consistency. The maximum horizontal principal stress is 1.81–1.95 times larger than the vertical stress, while the minimum horizontal principal stress is 0.98–1.03 times larger than the vertical stress. This can provide horizontal stress support for roadway horizontal deformation.

2.2. Roadway-Surrounding Rock Characteristics and Support

2.2.1. Roadway-Surrounding Rock Characteristics. According to the coal lithology exposed by drilling holes in the mining area, direct roof of the No. 3 coal is 8.5 m medium sandstone, which is gray and of poor sorting. The main roof is 16.2 m fine sandstone, with gray-white and wave bedding. The direct bottom is 2.8 m mudstone that is rich in plant fossils. The main bottom is 3.2 m medium-fine sandstone, which is light gray and contains mica and cuttings. Figure 3 lists the rock properties of the No. 3 coal seam roof and floor.

2.2.2. Roadway Support Parameters. The No. 3401 working face roadway haulage is a rectangular section. The roadway section width is 5.5 m, and the roadway height is 4.0 m. Table 2 lists the roadway support parameters, while Figure 4 shows the roadway support section.

2.3. Roadway Floor Heave. To monitor microseismic and rock burst events during the excavation, the high-precision SOS microseismic monitoring system was adopted in the mine. Figure 5 shows the structure of monitoring system, and Figure 6 shows the microseismic energy distribution of roadway during roadway haulage excavation.

Figure 6 shows that during August 4 to 12, the early excavation stage for roadway was influenced by horizontal tectonic stress and excavation disturbance. Microseismic events occurred frequently, but relatively little energy was released; this was considered the energy accumulation period. During August 13 to 29, microseismic events were in the active stage and the significantly increased energy was released, with the roadway constantly advancing in the anticlinal axis. During August 30 to September 8, the energy released by microseismic events increased further and the roadway started exhibiting dynamic stress phenomenon when excavation reached 160 m. Three roadway floor rock burst events were recorded during this period. However, the

	Drill hole	Rock stratum	Thickness (m)	Lithologic characteristics of rock
Roof		Medium-fine sandstone	7.32	Light gray, uniform bedding, hard, containing mica and cuttings
		Mudstone	5.4	Dark gray, rich in plant fossils, horizontal texture
		Fine sandstone	16.2	Gray-white, wavy bedding, containing mica and cuttings
Coal		Medium sand stone	8.5	Gray, poorly sorted, thin layer of calcareous sandstone
		No.3 coal	4.7	Black, weak bitumen luster, mixed port, dark and bright coal
Floor		Mudstone	2.8	Dark gray, rich in plant fossils, horizontal texture
		Medium-fine sandstone	3.2	Light gray, uniform bedding, hard, containing mica and cuttings
		Fine sandstone	5.64	Gray-white, wavy bedding, containing mica and cuttings
		Siltstone	12.3	Light grey, flaser bedding, local ingredients, semihard

Figure 3: No. 3 coal seam roof and floor lithology.

Table 2: Roadway support parameters.

	Interval distance (mm)	Length (mm)	Diameter (mm)	Roof anchor (cable)/root number	Roadway-side anchor/root number	Anchor (cable) material	Remarks
Anchor	1000 × 1000	2400	22	6	4	Thread steel	1 ∗ 19 core steel strand is used for anchor cable
Anchor cable	2000 × 2300	7200	21.6	3	0	Steel strand	

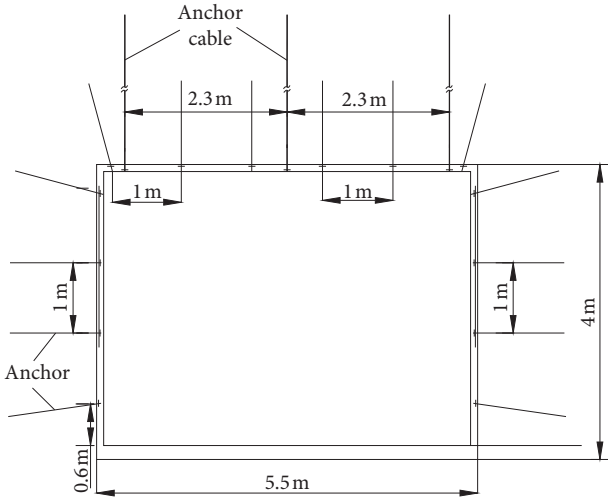

Figure 4: Layout of roadway support section.

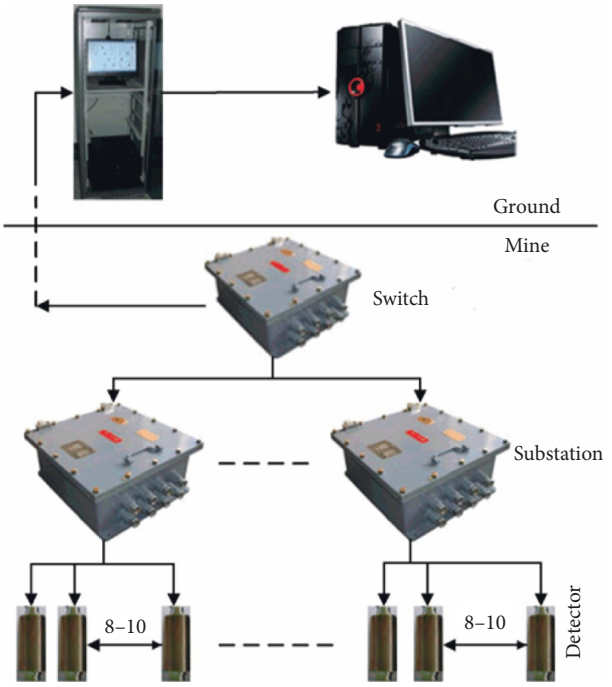

Figure 5: Microseismic monitoring system structure.

roadway roof and sidewalls had no obvious damage and maintained their integrity. Figure 7 shows the deformation and destruction of roadway-surrounding rock. These findings indicated the significance of studying roadway floor rock burst induced by mining disturbance, such as excavation disturbance and roof movement, to ensure mine safety.

3. Theoretical Analysis of Roadway Floor Stability

After excavation, deformation and damage of the roadway floor is mainly caused by horizontal stress and floor rock burst can easily occur [10]. The roadway floor's width is recorded as L with the unit length to analyze the stress, as shown in Figure 8(a). The stress analysis of floor deformation is shown in Figure 8(b).

3.1. Criterion Analysis of Roadway Floor Deformation. Based on the theory of material mechanics, the formulas for floor rock beam deflection and energy are as follows:

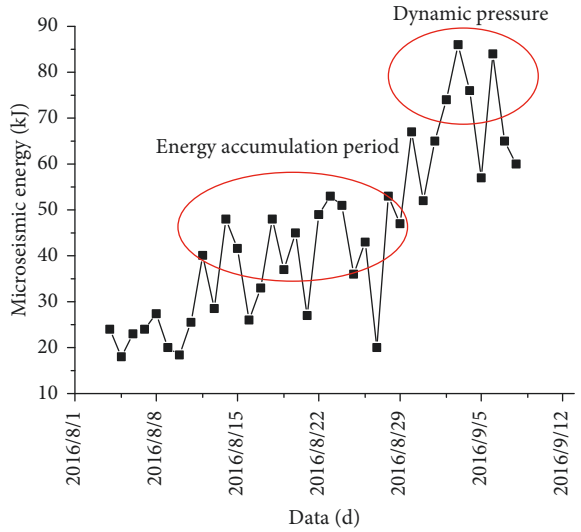

Figure 6: Microseismic energy distribution.

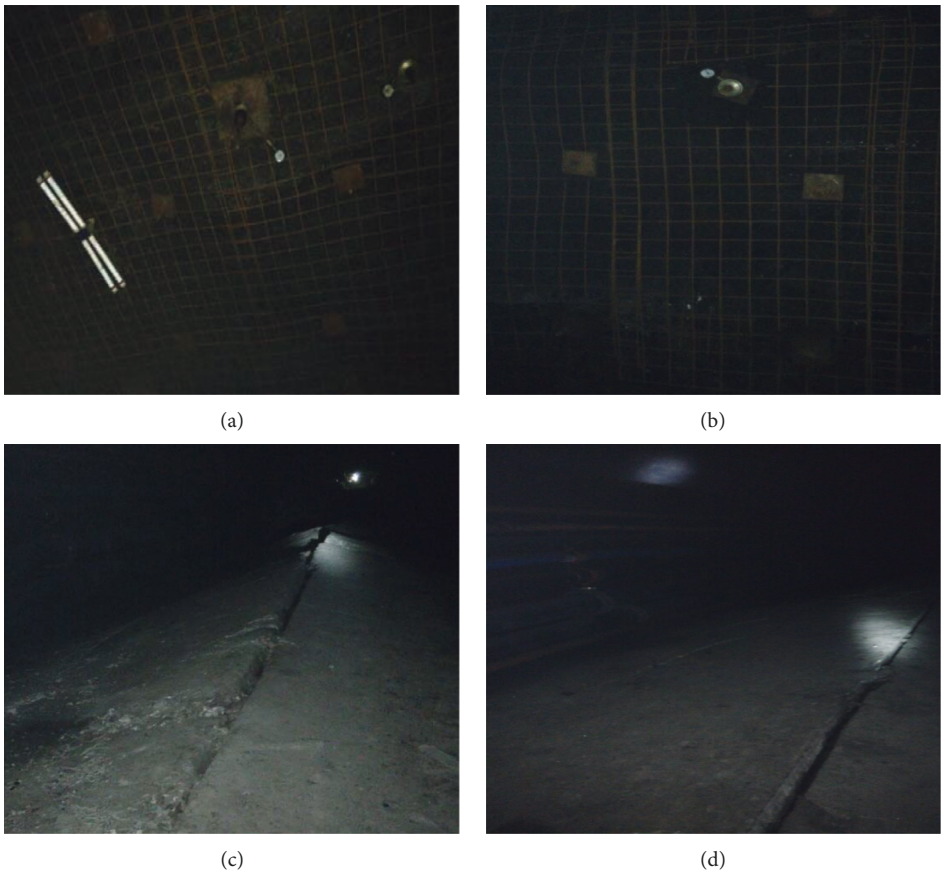

Figure 7: Deformation and failure of roadway-surrounding rock. (a) Roof. (b) Roadway side. (c) Floor. (d) Floor.

$$\frac{d^2w}{dx^2} = \frac{M(x)}{EI} = \frac{F\omega}{EI} + \frac{M_0}{EI}, \tag{1}$$

$$EI\frac{d^2w}{dx^2} = M, \tag{2}$$

$$dV_\varepsilon = \frac{M^2(x)}{2EI}dx, \tag{3}$$

where ω is the deformation of roadway floor, F is the roadway floor horizontal force, E is the elastic modulus of floor rock, I is the moment of inertia of floor rock, EI is the

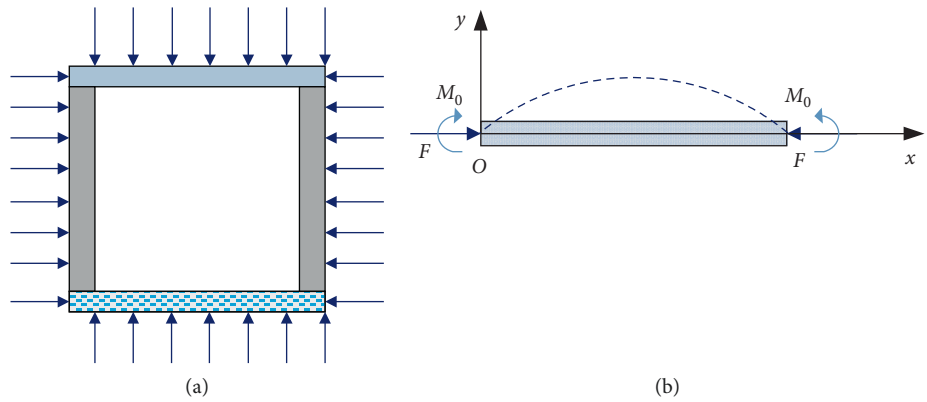

Figure 8: Simplified model of the roadway floor force. (a) Stress analysis of roadway-surrounding rock. (b) Stress analysis of floor deformation.

rock beam stiffness, M_0 is the rock beam moment, and dV_ε is the unit rock beam energy.

k is introduced to simplify the calculation:

$$k^2 = \frac{F}{EI}. \tag{4}$$

Equation (4) is substituted into equation (1):

$$\frac{d^2\omega}{dx^2} + k^2\omega = \frac{M_0}{EI}. \tag{5}$$

A general solution can be derived for equation (5):

$$\omega = A\sin kx + \cos kx + \frac{M_0}{F}, \tag{6}$$

where A and B are the integral constant terms of equation (5).

Using the stress analysis results for the floor rock beam, the initial condition of the beam can be deduced:

$$\begin{gathered} \omega(0) = 0, \\ \left.\frac{d\omega}{dx}\right|_{x=0} = 0, \\ \left.\frac{d\omega}{dx}\right|_{x=(l/2)} = 0, \\ \omega(l) = 0, \\ \left.\frac{d\omega}{dx}\right|_{x=l} = 0, \end{gathered} \tag{7}$$

where l is the roadway width.

Equation (7) is substituted into equation (6), and deflection is deduced as shown in the following equation:

$$\omega = \frac{M_0}{F}(1 - \cos kx), \tag{8}$$

where $k = 2n\pi/l$, $(n = 1, 2, 3, \ldots\ldots)$, is substituted into equation (4). The floor horizontal force is obtained as shown in the following equation:

$$F = \frac{4n^2\pi^2 EI}{l^2}, \tag{9}$$

where $n \in N^+$ indicates that the horizontal force F for maintaining floor rock stability beam has multiple values. Therefore, when $n = 1$, the horizontal force F reaches a minimum. That is, the minimum force F_{cr} is the critical stability force for the floor rock beam, as shown in the following equation:

$$F_{cr} = \frac{4\pi^2 EI}{l^2}. \tag{10}$$

The instability of the roadway floor rock beam $(F > F_{cr})$ can be determined using equation (10). The roadway floor has undergone bending deformation and even damage, thus deteriorating the safety and stability of the roadway.

3.2. Energy Analysis of the Roadway Deformation and Instability. In the process of roadway excavation, the laws of deformation and failure for surrounding rock are affected by mining dynamic disturbances such as blasting, roof movement, and adjacent working face mining, which can be distinguished from the surrounding rock under static loading.

Based on the law of thermodynamics, energy conversion is the essence of the physical change of the material. The deformation and failure of roadway floor can be attributed to four processes, namely, energy input, energy accumulation, energy dissipation, and energy release. In this article, the roadway floor rock burst is preliminarily discussed based on the energy principle, to provide a reference for other researchers.

According to the attenuation law for dynamic stress wave propagated in rock [34], the energy input E_D of the dynamic stress wave to the roadway floor in the process of surrounding rock propagation is shown in the following equation:

$$E_D = E_{D0} - E_B = E_{D0}(r - r_0)^{-\eta}, \tag{11}$$

where E_{D0} is the initial energy value at the earthquake center, and it can be obtained by using a microseismic monitoring system. E_B is the energy attenuated by stress wave in the process of propagating on the roadway floor. η is the stress wave attenuation coefficient, which is determined from the properties of rock mass. r and r_0 are, respectively, expressed as the radius of roadway and the earthquake source distance from the roadway center.

Equations (1)–(3) and (6) are combined, and accumulated strain energy expression for the microsection of the rock beam is as follows:

$$dV_\varepsilon = \frac{4n^4\pi^4 M_0^2 EI}{F^2 l^4}\left(1 + \cos\frac{4n\pi}{l}x\right)dx. \tag{12}$$

Based on the minimum energy principle of rock failure, energy released from the roadway-surrounding rock is bigger than the energy consumed in a rock burst [35]. The energy criterion for rock impact instability can be derived as follows:

$$E_c = \frac{\sigma_c^2}{2E}, \quad \text{or } E_c = \frac{\tau_c^2}{2E}, \tag{13}$$

$$E_0 = \int dV_\varepsilon + E_D - E_c > 0, \tag{14}$$

where E_0 is the residual elastic energy, E_D is the roadway-surrounding energy, and E_C is the energy consumed by rock mass destruction. σ_c and τ_c are, respectively, expressed as the uniaxial compressive strength and shear strength, while E is the rock mass elastic modulus.

Equations (11)–(14) are combined, and the energy criterion for a rock burst is deduced as shown in the following equation:

$$E_0 = \frac{4n^4\pi^4 M_0^2 EI}{F^2 l^4}\int\left(1 + \cos\frac{4n\pi}{l}x\right)dx + E_{D0}(r - r_0)^{-\eta} - \frac{\sigma_c^2}{2E} > 0. \tag{15}$$

According to equation (15), the residual energy E_0 of roadway floor is closely related to the bending moment M and its location, which are influenced by the roadway buried depth h, roadway span l, horizontal force F, and rock stiffness EI. When the roadway span l, rock stiffness EI, elastic modulus of rock E, and Poisson's ratio v are constant, the greater the roadway buried depth and dynamic load strength, the greater the residual elastic energy of the roadway floor, accompanied by the development and penetration of fractures. If the elastic energy is released instantaneously, rock burst can occur in the roadway floor, which will endanger safe and efficient mine production.

4. Analysis of Failure Characteristics and Causes of Rock Burst

4.1. Failure Characteristics of Roadway Floor Rock Burst

4.1.1. Borehole Detection Recorder Parameters. In light of the roadway haulage floor heave, the YTJ20 borehole detection recorder was used to detect cracks and separation in the roadway-surrounding rock. The recorder uses a high-resolution color peeposcope and LCD display. It can work continuously for 12 hours, achieving real-time image display and recording and storage with small volume, light weight, and simple operation. The borehole detection recorder and its main parameters are as shown in Table 3 and Figure 9.

4.1.2. Borehole Detection Monitoring Scheme. According to construction situation for the roadway, three detection sections were set at a specific distance from the roadway heading face at 100 m, 150 m, and 200 m, labeled Sections A, B, and C. Four detection boreholes were arranged in each detection section: roof drilling, roadway sidewalls drilling, and floor drilling. The "+" detection method was used for the borehole detection layout, with 12 monitoring boreholes in total. Borehole detection section layout is as shown in Figure 10(a). The borehole diameter was 32 mm, and the drilling length was 7 m; each detection boreholes were arranged, as shown in Figure 10(b).

4.1.3. Analysis of the Detection Results. The borehole detection recorder was used to detect the rock surrounding each detection section. At the same time, the section 80 m away from the roadway head was taken as the base level for avoiding surrounding rock rupture, on August 11, 2016. The roadway excavation speed was 10 m/d, and sequence of borehole detection is shown in Table 4.

After the detection was completed, video capture of the roadway roof, sidewalls, and floor was extracted as shown in Figures 11–13.

By using the borehole recorder to detect destruction of roadway-surrounding rock, fracture distribution of the surrounding rock was analyzed. An ultrasound transmitter was used to detect failure destruction in the surrounding rock between adjacent boreholes. Main parameters of mine ultrasonic transmitter are shown in Table 5 and Figure 14. The transmitter-monitoring point was identical with the borehole point. Firstly, borehole detection was carried out. Secondly, transmitter detection was carried out without rearranging the measuring points. Finally, rupture of surrounding rock occurred along the borehole from the outside to inside. The fracture area between adjacent boreholes was connected by using a spline curve, and the area between fracture areas was regarded as the complete area, as shown in Figure 15.

Figure 15 shows that the fracture area of roadway-surrounding rock gradually narrowed from its width along the borehole axis direction. The closer the detection section is to the anticline axis, the more serious the fracture in the surrounding rock. Sections A, B, and C in the roadway can be divided into two, two, and three fracture areas, respectively. Roadway-surrounding rock damage was most serious in the range of 1 m-2 m. The damage was mainly breakage and fracturing, and the scope was called the loose area. The second fracture circle was 3 m–4.5 m and mainly

Table 3: Main parameters of the YTJ20 borehole detection recorder.

Camera diameter (mm)	Camera length (mm)	Depth of detection (m)	Host size (length × width × height) (mm^3)	Working hours (h)	Storage capacity (G)
25	100	20	240 × 190 × 83	8	2

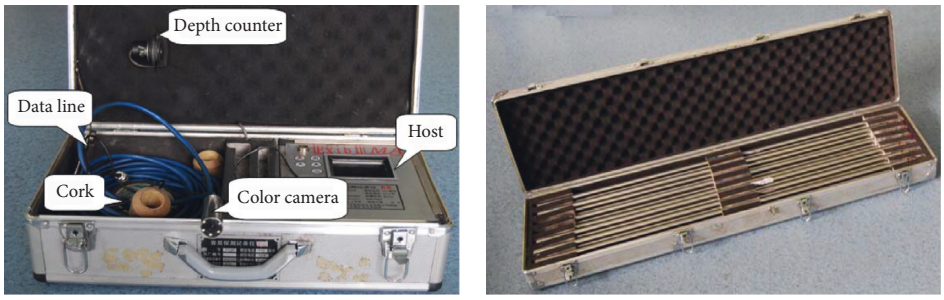

(a) (b)

Figure 9: YTJ20 borehole detection recorder. (a) Detection recorder host. (b) Guide rod.

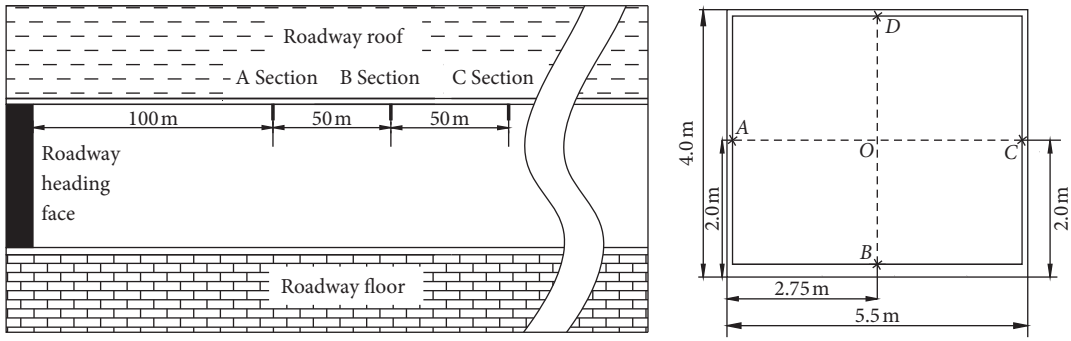

(a) (b)

Figure 10: Schematic diagram of detection section site layout.

Table 4: Detection sequence of roadway boreholes.

Time	Section number
August 21, 2016	A section
August 26, 2016	B Section
August 31, 2016	C Section

consisted of cracks and fissures. Along the borehole, the third fracture circle was 5.5 m–6 m. Sections A and B had only a few cracks in the roadway-surrounding rock. In addition, the fracture distribution for roadway floor was more serious than the distribution for roadway roof and sidewalls based on comparison of the roadway-surrounding fracture.

4.2. Cause Analysis of Roadway Floor Rock Burst. For causes of roadway floor failure, first, from roadway rock lithology perspective, the roadway roof is 24.7 m thick sand, while the floor is 2.8 m sandy mudstone with low bearing capacity. Second, from the perspective of roadway supporting measures, the roadway roof and sidewalls were supported by anchor, anchor cable, and wire mesh. However, the floor was unsupported, which resulted in low floor resistance to deformation and damage. Finally, based on the stress state of roadway-surrounding rock, the roadway was excavated in the anticlinal area, which made the surrounding rock change from three-dimensional stress state to two-dimensional stress state. The roadway roof and sidewalls were supported and retained the three-dimensional stress state, while the roadway floor had a two-dimensional stress state without support. Furthermore, roadway-surrounding rock was influenced by high tectonic stress and excavation disturbance stress, which further aggravated the floor failure.

5. Roadway Floor Rock Burst Control Technology

5.1. Design of Floor Rock Burst Control Technology. Based on the stability analysis and failure characteristics of roadway-surrounding rock, the integrity and stability of roadway roof and sidewalls can be maintained by using the original support parameters. Therefore, the roadway support design was only implemented for the roadway floor. The "overbreaking-bolting and grouting-backfill" method was put forward for controlling roadway floor

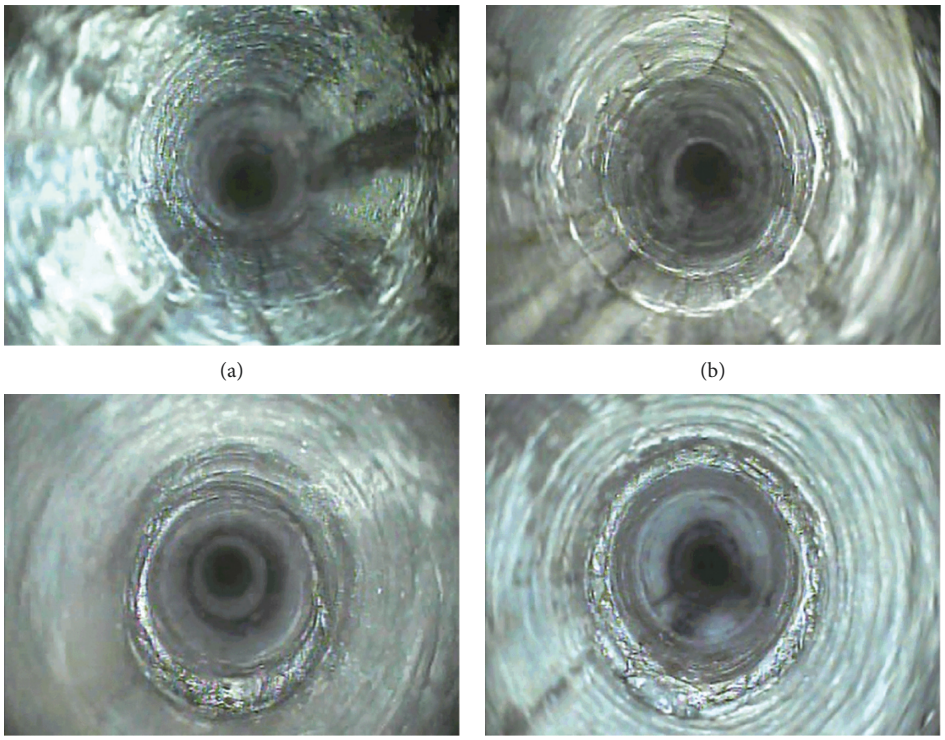

(a) (b)

(c) (d)

Figure 11: Video capture of the roof detection borehole. (a) Intact roof strata. (b) Fracture. (c) Crack. (d) Broken.

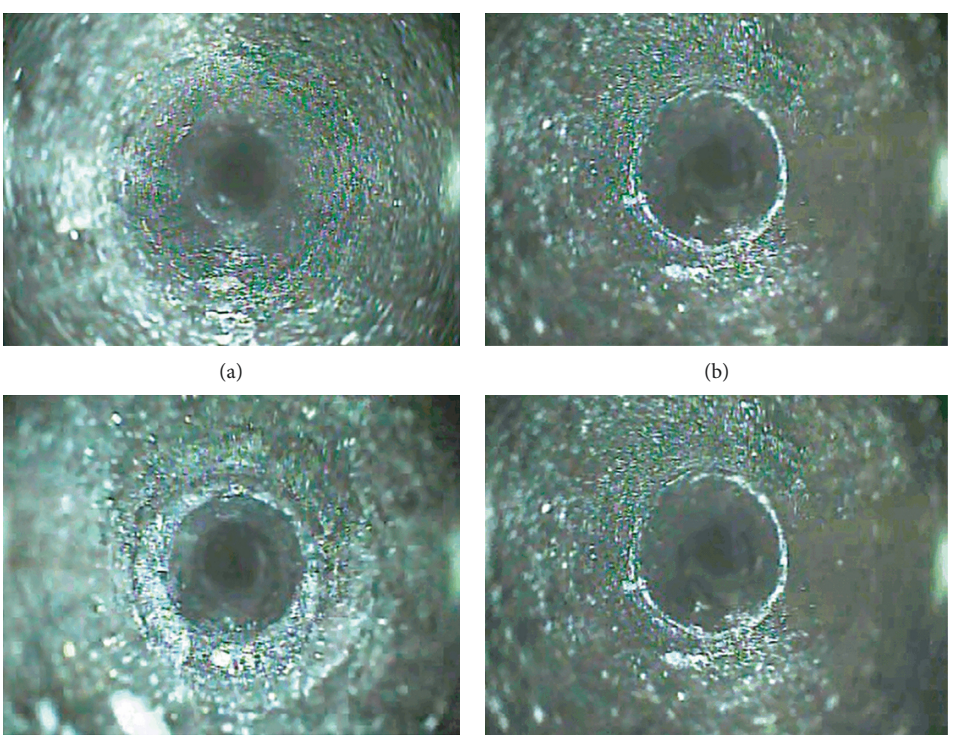

(a) (b)

(c) (d)

Figure 12: Video capture of the roadway side detection borehole. (a) Complete coal seam. (b) Fracture. (c) Crack. (d) Broken.

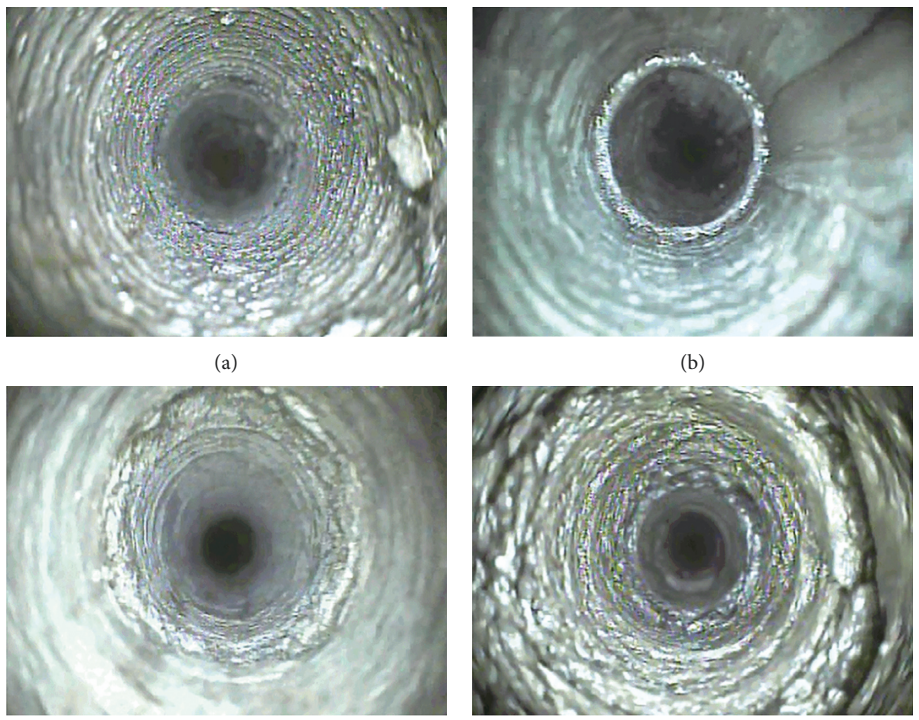

Figure 13: Video capture of the roadway floor detection borehole. (a) Complete floor rock stratum. (b) Fracture. (c) Crack. (d) Broken.

Table 5: Main parameters of the mine ultrasonic transmitter.

Host size (length × width × height) (mm^3)	Channel number	Ultrasonic time accuracy ($\mu\varepsilon$)	Working hours (h)	Transmitting voltage (V)	Storage capacity (G)
270 × 220 × 75	4	0.05	>5	65,250,500,1000	4

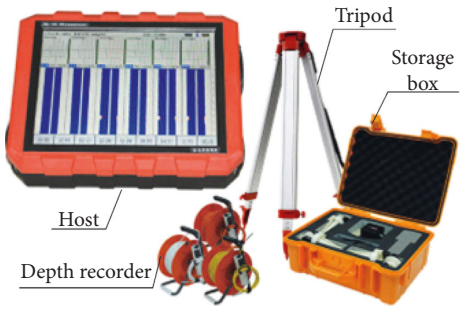

Figure 14: Mine ultrasonic transmitter.

rock burst, while the support parameters for roadway roof and sidewalls remain unchanged. The support parameters optimization processes for the roadway are shown in Figures 16 and 17.

The main support parameters for the roadway floor were as follows:

(1) Roadway floor overbreak

Rock mass from within 600 mm below the roadway floor was excavated, as shown in Figure 17(a).

(2) Grouting bolt

After excavation, the left-lateral and high-strength grouting bolts were used to support the roadway floor. The specification of bolt was Φ25 mm × 2,400 mm, and the bolt spacing was 1,000 mm, corresponding to the position of roof bolts, as shown in Figure 17(b). The grouting pressure was 2.3 MPa–3.4 MPa.

(3) Concrete grouting

After grouting bolt installation, the roadway floor was grouted with the thickness 20 mm of spray layer, for maintaining smoothness and integrity of the floor, and the grouting port of bolt should be protected to prevent blockage.

(4) Grouting slurry

The PO42.5 alumino-silicate cement single slurry was selected as the grouting material, and the water-cement ratio was 1 : 2.5.

(5) Concrete backfilling

Concrete of strength grade C40 was used to backfill the overbreak portion of roadway floor, as shown in Figure 17(c).

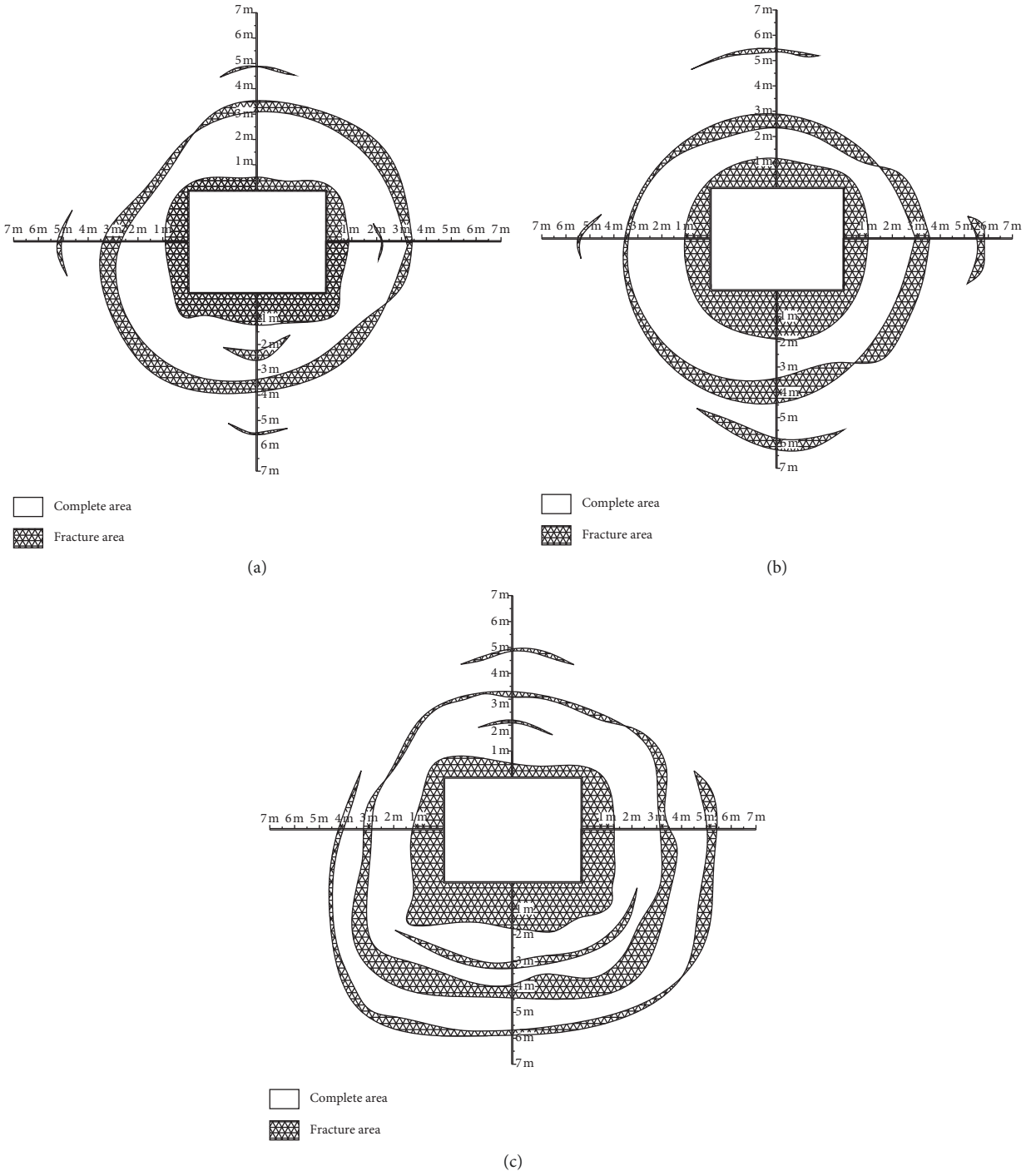

Figure 15: Fracture distribution of the roadway-surrounding rock. (a) A Section. (b) B Section. (c) C Section.

In addition, according to roadway's actual excavation situation for the roadway, reinforcement of the roadway floor was carried out 50–70 m behind the roadway working face.

According to the above steps, improved floor lithology can effectively alleviate the floor's stress effect. The cracked rock can be cemented by grouting, and the integral bearing capacity of roadway floor will thus be enhanced.

5.2. Field Application. Deformation of the roadway in the test section was monitored for three months to evaluate the support effect of the roadway floor optimization scheme. The monitoring content included roof subsidence, floor heave, and displacement of the roadway sidewalls. The measuring point of roadway-surrounding rock was arranged using the "+" measuring method. Monitoring points *A* and *C* were located at 1.375 m from the roadway floor to roadway side. Monitoring

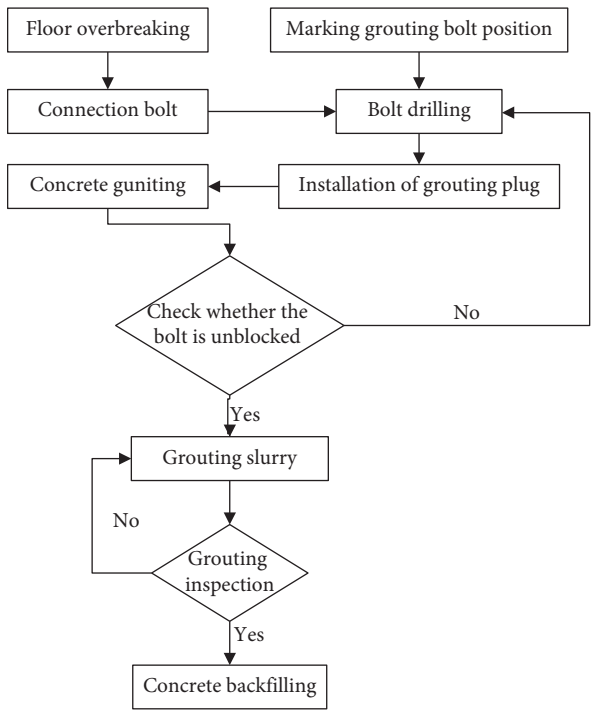

Figure 16: Construction flowchart of the roadway floor.

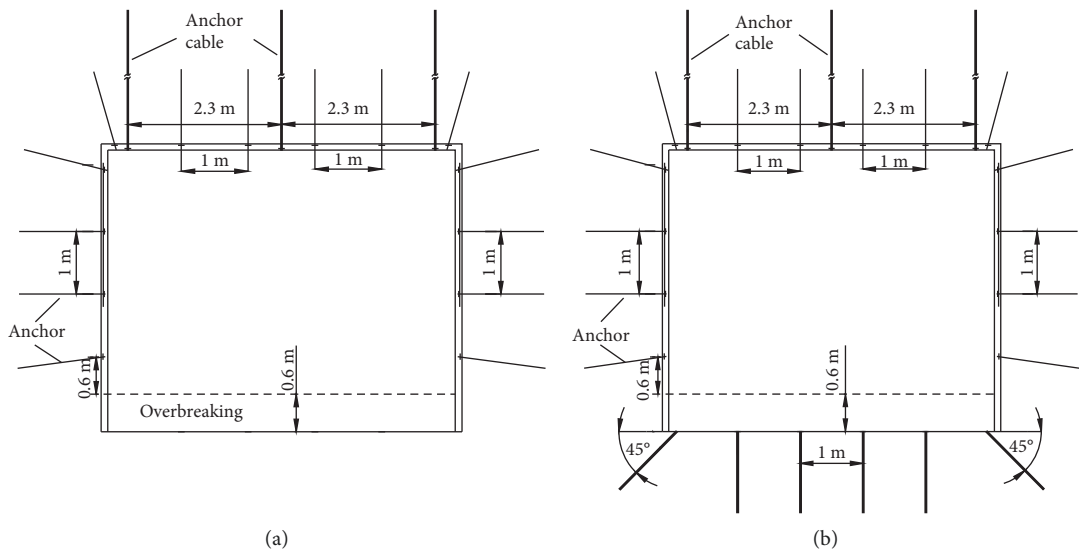

Figure 17: Continued.

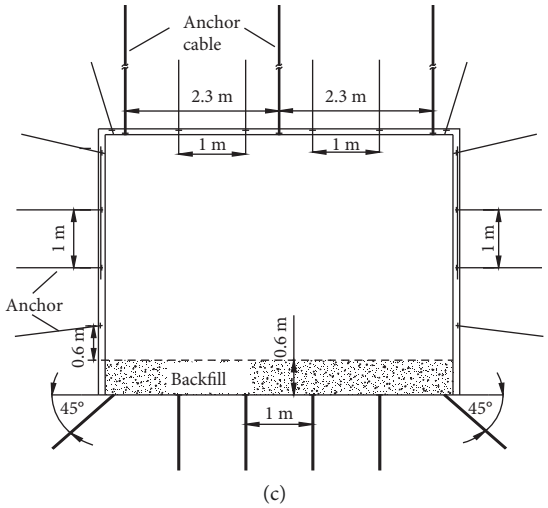

Figure 17: Roadway support parameter optimization design diagram. (a) Overbreaking. (b) Bolting and grouting (c) Backfill.

point B was located at 2.75 from the floor to roadway side. Monitoring points D and D_1 were located at 2.0 m from the roadway side to floor, as shown in Figure 18.

Based on monitoring deformation data for the roadway-surrounding rock, deformation distribution of the roadway-surrounding rock was plotted as shown in Figure 19.

Figure 19 showed that the deformation of roadway-surrounding rock entered into an active phase after excavation. Roof subsidence, convergence deformation of the roadway sidewalls, and floor heave were more obvious. When the distance between reinforcing position of the floor and roadway working face was 50–70 m, overbreaking, grouting, and backfilling started occurring, and the lithology of roadway floor improved with roadway excavation. After grouted support of the roadway floor, the floor's deformation rate gradually changed from 1.3 mm/d to 0.33 mm/d. The roadway floor deformation changed from the rapid deformation phase to slow deformation phase, and the deformation eventually stabilized. The floor lithology also had a better control effect on the deformation of the roadway roof and sidewalls, thus guaranteeing stability and safety of the roadway-surrounding rock. The support effect of roadway after optimizing the support parameter is shown in Figure 20. The distribution of roadway microseismic energy during excavation ifs shown in Figure 21.

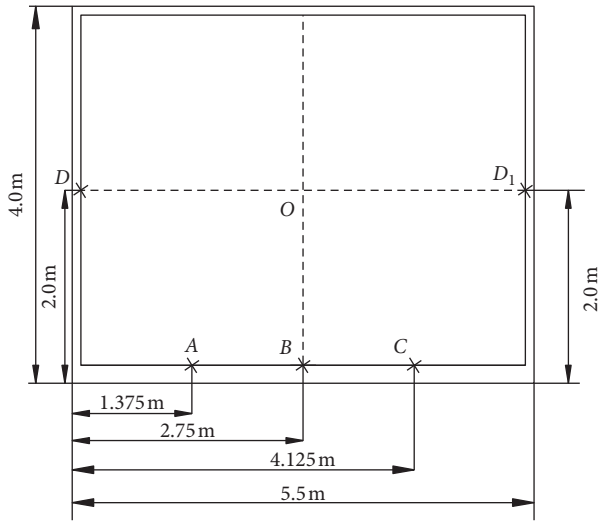

Figure 18: Monitoring point layout for the roadway surface.

6. Results

This article analyzed the deformation and failure characteristics of roadway-surrounding rock based on the roadway floor deformation induced by floor rock burst. Then, the "overbreaking-bolting and grouting-backfill" method was put forward to prevent roadway floor rock burst and heave and to guarantee roadway stability. The main results obtained were as follows:

(1) Deformation instability criterion for the roadway floor was deduced using the theory of material mechanics. The energy transformation of floor rock burst was discussed preliminarily using the energy conservation principle. We concluded that the greater the depth and dynamic load of the roadway, the greater the floor elastic energy storage, thus increasing the likelihood of a roadway floor rock burst.

(2) Using a borehole recorder to determine the internal characteristics of roadway-surrounding rock, the fractured area in the roadway-surrounding rock was found to narrow gradually in terms of its width along the borehole axis direction. The closer the detection section was to the anticlinal axis, the more the serious fracturing of the surrounding rock. In addition, the roadway floor contained many cracks and broken areas, whereas cracks and fissures occurred in the roadway roof and sidewalls.

(3) Based on the deformation and failure characteristics of deep roadways, the "overbreaking-bolting and

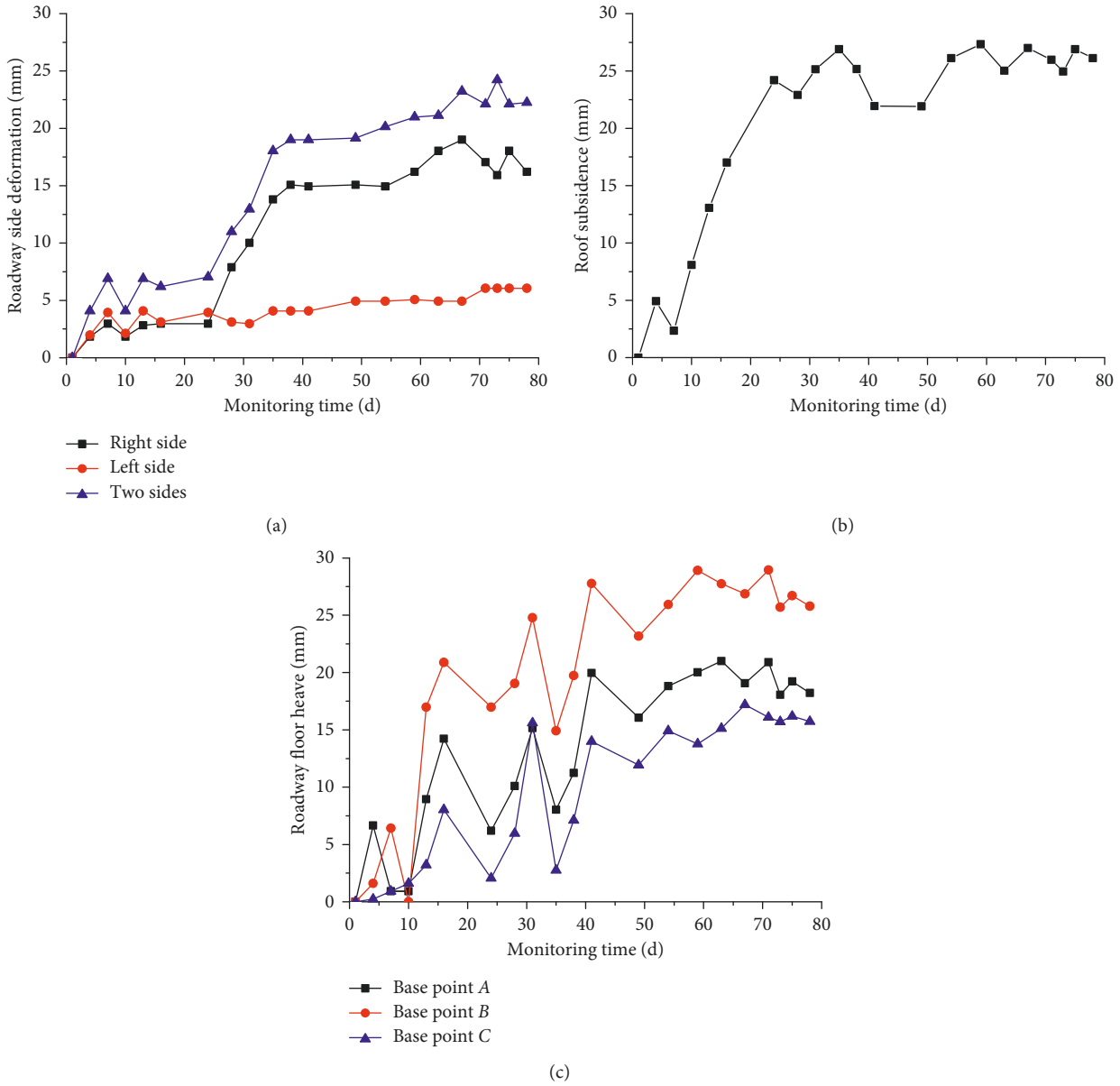

Figure 19: Displacement distribution curves of roadway-surrounding rock. (a) Roadway sides. (b) Roof. (c) Floor.

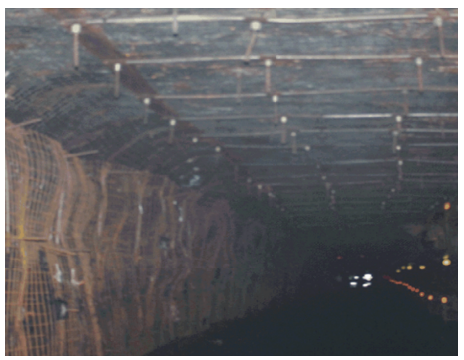

Figure 20: Roadway support parameters optimization effect.

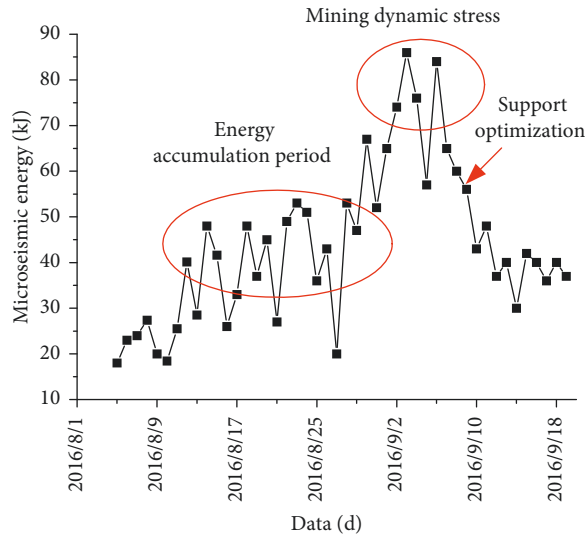

Figure 21: Distribution of roadway microseismic energy.

grouting-backfill" method was put forward and tested in the field. The results showed that the floor's deformation was effectively controlled and the total deformation was small, thus ensuring the stability of the roadway-surrounding rock.

Data Availability

The data used to support the findings of this study are available from the corresponding author upon request.

Conflicts of Interest

The authors declare that they have no conflicts of interest.

Authors' Contributions

Zhimin Xiao analyzed data and wrote the paper. Jun Liu and Shitan Gu contributed data and performed analysis of data. Mingqing Liu, Futian Zhao, Yue Wang, and Chen Ou contributed to field monitoring.

Acknowledgments

This work was supported by the National Natural Science Foundation of China (nos. 51874118, 51174076, and 51044003), the Fundamental Research Funds for the Central Universities (no. KYCX18-0567), the State Key Research Development Program of China (no. 2016YFC0801403), and the Shandong Provincial Natural Science Foundation, China (ZR2018MEE009).

References

[1] Y. L. Tan, *Ground Pressure and Strata Control*, China Coal Industry Publishing Home, Beijing, China, 2011.

[2] Q. X. Qi and L. M. Dou, *Theory and Technology of Rock Burst*, China University of Mining and Technology Press, Xuzhou, China, 2008.

[3] P. P. Prochazka, "Application of discrete element methods to fracture mechanics of rock bursts," *Engineering Fracture Mechanics*, vol. 71, no. 4–6, pp. 601–618, 2004.

[4] S. V. Tsirel and N. V. Krotov, "Probability interpretation of indirect risk criteria and estimate of rock burst hazard in mining Anthra cite seams," *Journal of Mining Science*, vol. 37, no. 3, pp. 240–260, 2001.

[5] J. F. Pan, Y. Ning, D. B. Mao, H. Lan, T. T. Du, and Y. W. Peng, "Theory of rockburst start-up during coal mining," *Chinese Journal of Rock Mechanics and Engineering*, vol. 31, no. 3, pp. 586–596, 2012.

[6] Y. D. Jiang and Y. X. Zhao, "State of the art: investigation on mechanism, forecast and control of coal bumps in China," *Chinese Journal of Rock Mechanics and Engineering*, vol. 34, no. 11, pp. 2188–2204, 2015.

[7] A.-X. Wu, Y.-Z. Sun, S. Gour, H.-M. Shen, and B.-H. Yang, "Characteristics of rockburst and its mining technology in mines," *Journal of Central South University of Technology*, vol. 9, no. 4, pp. 255–259, 2002.

[8] N. G. W. Cook, "The failure of rock," *International Journal of Rock Mechanics and Mining Sciences & Geomechanics Abstracts*, vol. 2, no. 4, pp. 389–403, 1965.

[9] N. G. W. Cook, E. Hoek, J. P. G. Pretorius et al., "Rock mechanics applied to the study of rock bursts," *Journal of the South African Institute of Mining and Metallurgy*, vol. 65, pp. 437–446, 1965.

[10] A.-Z. Hua and M.-Q. You, "Rock failure due to energy release during unloading and application to underground rock burst control," *Tunnelling and Underground Space Technology*, vol. 16, no. 3, pp. 241–246, 2001.

[11] A. Kidybiński, "Bursting liability indices of coal," *International Journal of Rock Mechanics and Mining Sciences & Geomechanics Abstracts*, vol. 18, no. 4, pp. 295–304, 1981.

[12] Y. Pan, Y. Liu, and S. Gu, "Fold catastrophe model of mining fault rock bust," *Chinese Journal of Rock Mechanics and Engineering*, vol. 20, no. 1, pp. 43–48, 2001.

[13] Y. Pan, "Discussion on "Fold catastrophe model of rock dynamic destabilization"," *Chinese Journal of Geotechnical Engineering*, vol. 32, no. 1, pp. 58–60, 2010.

[14] G. Z. Yin, H. Li, X. F. Xian, and F. Tao, "The catastrophic theory model of instability of coal and rock mass," *Journal of Chongqing University*, vol. 17, no. 1, pp. 23–28, 1994.

[15] H. P. Xie, Y. Ju, and L. Y. Li, "Criteria for strength and structural failure of rocks based on energy dissipation and energy release principles," *Chinese Journal of Rock Mechanics and Engineering*, vol. 24, no. 17, pp. 3003–3010, 2005.

[16] Q. X. Qi, T. Q. Liu, and Y. W. Shi, "Mechanism of fraction sliding disability of rock burst," *Ground Pressure and Strata Control*, vol. 3-4, pp. 174–177, 1995.

[17] N. J. Ma, X. F. Guo, Z. Q. Zhao et al., "Occurrence mechanisms and judging criterion on circular tunnel butterfly rock burst in homogeneous medium," *Journal of China Coal Society*, vol. 41, no. 11, pp. 2679–2688, 2016.

[18] T. Yang, E. C. Westman, B. Slaker, X. Ma, Z. Hyder, and B. Nie, "Passive tomography to image stress redistribution prior to failure on granite," *International Journal of Mining, Reclamation and Environment*, vol. 29, no. 3, pp. 178–190, 2015.

[19] B.-Y. Jiang, S.-T. Gu, L.-G. Wang, G.-C. Zhang, and W.-S. Li, "Strainburst process of marble in tunnel-excavation-induced

stress path considering intermediate principal stress," *Journal of Central South University*, vol. 26, no. 4, pp. 984–999, 2019.

[20] X. F. Xu, L. M. Dou, J. Liu et al., "Research of reasons and controlling for floor burst in coal mine roadway," *Rock and Soil Mechanics*, vol. 31, no. 6, pp. 1977–1982, 2010.

[21] S. T. Gu, Z. M. Xiao, B. Y. Jiang, R. Huang, and P. Shan, "Research of rock burst risk induced by mining and field case in anticlinal control area," *Advance in Civil Engineering*, vol. 2018, Article ID 2632549, 10 pages, 2018.

[22] F. X. Jiang, S. H. Yang, Y. H. Cheng et al., "A study on microseismic monitoring of rock burst in coal mine," *Chinese Journal of Geophysics*, vol. 49, no. 5, pp. 1511–1516, 2006.

[23] E. Y. Wang, X. Q. He, L. M. Dou, S.-N. Zhou, B.-S. Nie, and Z.-T. Liu, "Electromagnetic radiation characteristics and rocks during excavation in coal mine and their application," *Chinese Journal of Geophysics*, vol. 48, no. 1, pp. 216–221, 2005.

[24] Y. L. Tan, H. Zhou, X. J. Han et al., "Analysis on acoustic emission pattern for rock burst," *Chinese Journal of Rock Mechanics and Engineering*, vol. 19, no. 4, pp. 425–428, 2000.

[25] S. Husen, E. Kissling, and A. von Deschwanden, "Induced seismicity during the construction of the Gotthard Base Tunnel, Switzerland: hypocenter locations and source dimensions," *Journal of Seismology*, vol. 17, no. 1, pp. 63–81, 2013.

[26] Y. X. Zhao, Y. D. Jiang, T. Wang, G. Feng, and X. Shuai-Tao, "Features of microseismic events and precursors of rock burst in underground coal mining with hard roof," *Journal of China Coal Society*, vol. 37, no. 12, pp. 1960–1966, 2012.

[27] A.-Y. Cao, L.-M. Dou, C.-B. Wang, X.-X. Yao, J.-Y. Dong, and Y. Gu, "Microseismic precursory characteristics of rock burst hazard in mining areas near a large residual coal pillar: a case study from Xuzhuang coal mine, Xuzhou, China," *Rock Mechanics and Rock Engineering*, vol. 49, no. 11, pp. 4407–4422, 2016.

[28] X. Q. He, B. S. Nie, E. Y. Wang et al., "Electromagenetic emission forecasting technology of coal or rock dynamic disasters in mine," *Journal of China Coal Society*, vol. 32, no. 1, pp. 56–59, 2007.

[29] Y. S. Pan, Y. H. Xiao, Z. H. Li, and K.-X. Wang, "Study of tunnel support theory of rock burst in coal mine and its application," *Journal of China Coal Society*, vol. 39, no. 2, pp. 222–228, 2014.

[30] H. P. Kang, Y. Z. Wu, J. He et al., "Rock bolting performance and field practice in deep roadway with rock burst," *Journal of China Coal Society*, vol. 40, no. 10, pp. 2225–2233, 2015.

[31] Z.-L. Li, L.-M. Dou, W. Cai, G.-F. Wang, Y.-L. Ding, and Y. Kong, "Roadway stagger layout for effective control of gob-side rock bursts in the longwall mining of a thick coal seam," *Rock Mechanics and Rock Engineering*, vol. 49, no. 2, pp. 621–629, 2016.

[32] D. Raju, H. Mitri, and D. Thibodeau, "Mine safety enhancement by designing dynamic rock supports," *Procedia Engineering*, vol. 26, pp. 1591–1602, 2011.

[33] G. R. Feng, P. F. Wang, Y. P. Chugh, J. Zhao, Z. Wang, and Z. Zhang, "A coal burst mitigation strategy for tailgate during deep mining of inclined longwall top coal caving panels at Huafeng coal mine," *Shock and Vibration*, vol. 2018, Article ID 5929785, 18 pages, 2018.

[34] Y. S. Zhao, Z. C. Feng, and Z. J. Wan, "Least energy principle of dynamical failure of rock mass," *Chinese Journal of Rock Mechanics and Engineering*, vol. 23, no. 11, pp. 1781–1783, 2003.

[35] M. S. Gao, L. M. Dou, N. Zhang, Z. L. Mu, K. Wang, and B. Yang, "Experimental study on earthquake tremor for transmitting law of rock burst in geomaterials," *Chinese Journal of Rock Mechanics and Engineering*, vol. 26, no. 7, pp. 1365–1371, 2007.